Title

Density functional theory assessment of the lithiation thermodynamics and phase evolution in si-based amorphous binary alloys

Authors

Sivonxay, Eric

Persson, Kristin A

Publication Date

2022-12-01

DOI

10.1016/j.ensm.2022.08.015

Energy Storage Materials 53 (2022) 42–50

Contents lists available at ScienceDirect

Energy Storage Materials

journal homepage: www.elsevier.com/locate/ensm

Density functional theory assessment of the lithiation thermodynamics and phase evolution in si-based amorphous binary alloys

Eric Sivonxay [a,b], Kristin A. Persson [*,a,b,c]

[a] Energy Technologies Area, Lawrence Berkeley National Laboratory, Berkeley, California 94720, United States
[b] Department of Materials Science, University of California Berkeley, Berkeley, California 94720, United States
[c] The Molecular Foundry, Lawrence Berkeley National Laboratory, Berkeley, California 94720, United States

ARTICLE INFO

Keywords:
Li-ion batteries
Theory and modeling
Alloys
Si anodes

ABSTRACT

Development of novel alloy-based anodes has the potential to increase the energy storage capacity of current Li-ion based energy storage technology. In particular, Si-based anodes are of interest due to their high theoretical capacity, but suffer from poor cycle and calendar life stemming from large volumetric expansion and a non-passivating solid-electrolyte interface. The addition of amorphous components to the Si anode has been shown to improve the mechanical and chemical stability during lithiation. In this study, we use density functional theory (DFT) to probe the thermodynamics of amorphous alloy formation in a range of binary Si-X alloy systems, where X constitutes any element from periodic table groups 1–17. The alloying elements are classified as active or inactive components based on the reactivity with Li, where active elements form stable binary compounds with Li and inactive elements do not. We find that when alloying inactive elements, most inactive components do not fully reduce and hence result in the extrusion of metallic phases. Formation of Si-X compounds with no reactivity to Li results in deactivation of Si and decreased capacity. Alloying with Li-inactive elements also bypasses early Si lithiation stages and decreases the onset potential for lithiation. Most of the Li-active elements do not form stable Si-X binaries or Li-Si-X ternaries, resulting in lithiation potentials composed of voltage steps matching those of the base elements (Li_xX and Li_xSi), while the others may not be of much practical use due to their high lithiation potentials or preciousness, but may buffer against volumetric expansion.

1. Introduction

Lithium-ion secondary batteries are currently the dominant energy storage technology for consumer electronic devices and are increasingly in demand as the adoption of electric vehicles and renewable energy rises [1–3]. Current generation Li-ion batteries, utilizing graphite intercalation materials, are nearing their limits for energy storage, and continued improvements in negative electrode energy density require the transition to alternative anode materials [4]. Silicon has been suggested as a replacement for graphite in Li-ion batteries due to its high theoretical capacity in conjunction with its high abundance and global production. Amorphous Si delivers up to 3579mAhg^{-1} when cycled at room temperature. However, concurrently Si suffers from electrode performance degradation resulting from the significant volumetric expansion associated with Li alloying [5–8] as well as the formation of an unstable solid electrolyte interphase (SEI) which leads to continuous electrolyte decomposition and loss of Li inventory [9,10]. Strategies to mitigate volumetric expansion primarily involve nanostructuring to introduce void space, allowing for particle swelling and reducing internal stress during cycling [5,11]. However, nanostructuring also accelerates electrolyte reduction by increasing the contact area between the active material and electrolyte, resulting in low initial coulombic efficiency [12]. Amorphous Si has yielded marked improvement in mechanical stability due to the absence of phase separation during lithiation, reducing stress originating from phase boundaries between distinct lithiated phases [13]. Attempts to promote the formation of a suitable SEI have found improved capacity retention and extended cycle life but still fall short of requirements for commercial application [14,15]. Alloying Si with other elements is another effective strategy to mitigate volume expansion and modify SEI formation by modulating lithiation voltage, volumetric expansion, surface reactivity, and phases formed during cycling [16–19].

Alloyed elements are either active or inactive depending on their reactivity with Li. Elements that form stable binary phases with Li (such as Si, Ge, Sn, and Sb) are considered active, while those that do not form

* Corresponding author.
E-mail address: kapersson@lbl.gov (K.A. Persson).

https://doi.org/10.1016/j.ensm.2022.08.015
Received 2 February 2022; Received in revised form 29 July 2022; Accepted 9 August 2022
Available online 24 August 2022

stable binaries (e.g. Ti, Cr, Mn, and Ni) are deemed inactive [11,20]. The alloys of active elements have received much attention, as the electrochemical characteristics of alloyed active components can be markedly different from the individual elements [11,21]. Additionally, the presence of a third element in these glasses is associated with increased fracture toughness, leading to higher mechanical stresses during cycling which suppresses the formation of the crystalline $Li_{15}Si_4$ phase, which is known to contribute to electrode cracking and voltage hysteresis [13,22]. Although high stress from lithiation typically results in the fracturing of Si, amorphous materials such as metallic glasses exhibit higher yield strength, fracture toughness, and resistance to crystallization and may be capable of withstanding forces associated with lithiation [23–25]. While the alloying of inactive elements, especially at high concentrations, is detrimental to energy storage capacity, the inclusion of these components lowers the maximum volumetric expansion, similar to the inclusion of void space through nanostructuring [19]. Consequently, compared to a-Si with a depth of charge restricted to similar volumetric expansion, alloys yield a decreased average voltage and increased energy density.

While much work and several extensive reviews are devoted to the performance of Si-based alloy electrodes [11,20,26], most predictions of lithiation behavior use the known crystalline phases from the Materials Project [11,27,28]. While this approach may be sufficient in systems with high ionic diffusivity, such as Sn, which lithiate through a series of crystalline phases, ionic diffusivity in crystalline Si is sluggish and amorphization is pervasive [11,16]. Therefore, examining the crystalline polymorphs likely results in an incomplete picture of the systems, since only a handful of lithiated compositions are represented in the calculation set. An understanding of formation of binary Si alloys and their corresponding lithiated amorphous alloys is necessary when designing alloying and conversion electrodes. In this work, we present a comprehensive ab-initio study of the thermodynamics and lithiation characteristics of amorphous binary Si-X alloys and/or compounds. Although some elements may be unsuitable for use in Li-ion batteries due to their toxicity, high cost, or low abundance, we include these elements for completeness and comparison.

2. Computational methodology

2.1. Methods

For all elements investigated, we sampled amorphous structures using ab-initio molecular dynamics (AIMD) and Density Functional Theory (DFT), similar to previous work on the Li-Si and Li-Si-O systems [29]. High-throughput workflows were implemented in the mpmorph [30] software package using the atomate [31], fireworks [32], and pymatgen [33] python packages. A modification to the volume rescaling approach was necessary for robust and accelerated convergence of equilibrated liquid melts. Density convergence was achieved by running three parallel AIMD simulations with different densities, regression analyses of the Birch-Murnaghan EOS (shown in Eq. (1)), and identifying V such that $P(V) = 0$ [34,35].

$$P(V) = \frac{3B_0}{2}\left[\left(\frac{V_0}{V}\right)^{\left(\frac{7}{3}\right)} - \left(\frac{V_0}{V}\right)^{\left(\frac{5}{3}\right)}\right]\left\{1 + \frac{3}{4}\left(B_0' - 4\right)\left[\left(\frac{V_0}{V}\right)^{\left(\frac{2}{3}\right)} - 1\right]\right\} \quad (1)$$

All Density Functional Theory (DFT) calculations were performed using the Vienna Ab-initio Simulation Package (VASP) [36,37], with projector augmented-wave (PAW) potentials [38] along with the Perdew-Burke-Ernzerhof (PBE) generalized-gradient functional (GGA) [39] and the GGA+U extension [40] where applicable. The Python Materials Genomics (pymatgen) package was used to generate input files with calculation parameters (U values, convergence criteria etc) consistent with those of the Materials Project [27,33]. Structure optimizations were performed using the MPRelaxSet within pymatgen, with a plane wave energy cutoff of 520eV with a minimum reciprocal lattice density of 64 per per $Å^{-3}$. AIMD simulations utilized a plane-wave cutoff of 400 eV, one Γ centered k-point, and a time step of 2fs as documented in the MPMDSet.

2.2. Thermodynamic stability

Formation energy is used to compare the relative stability of compounds to their elemental constituents. The formation energy for the amorphous and crystalline phases is calculated with respect to the crystalline phases according to Eq. (2).

$$U_F\left(Li_nSi_{1-n-y}X_y\right) = U\left(Li_nSi_{1-n-y}X_y\right) - nU(\mathrm{c-Li}) - (1-n-y)U(\mathrm{c-Si}) - yU(\mathrm{c-X}) \quad (2)$$

To evaluate the relative stability of the crystalline phases available in the Materials Project [27], a ternary phase diagram was generated for each chemical system. The phase diagram is constructed from the convex hull of composition and formation energy (U_F), such that phases coincident with the hull represent thermodynamically stable equilibrium phases [41] at low temperatures. Tie-lines, or line segments, connecting two stable points represent a two-phase equilibrium, such that materials with composition falling on the tie line will be predisposed to decomposing to form the bounding phases. Likewise, tie-triangles correspond to three-phase equilibria, where materials with formulas coincident with the triangles are composed of the phases at the vertices.

In addition to the construction of the crystalline phase diagram, we compose a hull for the amorphous phases. As there exists no well defined amorphous structure, an ensemble of ten amorphous structures are sampled and their formation energies are averaged. Structures are sampled uniformly in time from a 10ps AIMD simulation at 4000K, with samples corresponding to DFT relaxation of the simulation cells observed at 1, 2, 3, ..., 9, and 10ps. An analysis of the distribution of formation energies is shown in Fig. S1. The amorphous convex hull is constructed in similar manner to the crystalline phase diagram, however all the crystalline energies are omitted except for BCC Li. In the absence of long and medium-range order and insufficient kinetic energy to overcome barriers for structural reorganization, decomposition into stable crystalline phases will be slow and the amorphous hull may be used to predict the lithiation behavior of Si-X alloys. Employing anode alloys that do not react with Li tends to result in Li metal plating, which motivates the use of the BCC polymorph as a reference state for Li.

An example phase diagram is shown in Fig. 1 for a Li-Si-X system. Interpreting the lithiation pathway from the ternary phase diagrams follows a line segment connecting the composition with the pure Li point with considerations to the phase equilibria. A sample lithiation pathway is provided for a-XSi_4 (indicated by the yellow circle), which passes through the tie-triangles I, II, III, and IV, each corresponding to unique lithiation multi-phase stages for the material. In stage I, Li alloys with Si and extrudes XSi_2, quantities determined by applying the lever rule at the point of intersection with the XSi_2-LiSi tie line. Continued lithiation in stage II results in the displacement of XSi, a more X rich alloy, from XSi_2 and formation of more LiSi. In stage III, Li alloying converts LiSi into $Li_{15}Si_4$ with no change to XSi. Lithiation is bounded by stage IV since all present phases are in equilibrium with Li. Therefore, Li alloying is less favorable than Li plating at the electrode. Similar to stage IV, alloy formulations coincident with the XSi-X_4Si-Li (V) and X_4Si-X-Li (VI) phase equilibria are not expected to lithiate.

Extending from the convex hulls and phase diagram, the equilibrium lithiation potentials for crystalline and amorphous materials are predicted [29,42]. As a summary, the lithium chemical potentials are determined for each three-phase equilibria in the crystalline phase diagram and amorphous convex hull. The Li chemical potentials are then related to the potential, E, by Eq. (3).

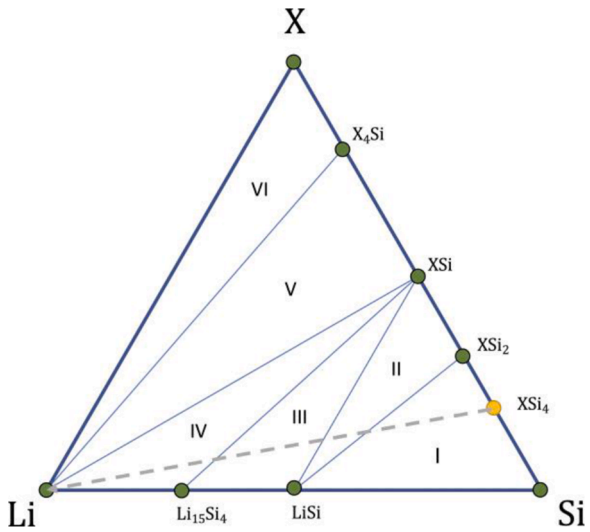

Fig. 1. Example phase diagram for a Li-Si-X ternary system with all 3-phase equilibrium regions labeled. Stable phases are noted by green circles. Lithiation pathway of XSi_4 (marked in yellow) is drawn with a dashed grey line. (For interpretation of the references to colour in this figure legend, the reader is referred to the web version of this article.)

$$\mu_{Li} - \mu^0_{Li} = neE \tag{3}$$

where μ_{Li} is the chemical potential of Li within the lithiated phase, μ^0_{Li} is the reference chemical potential of BCC Li metal, e is the elementary charge of an electron, and n is the moles of Li inserted per mole of the host.

The estimated full stack energy (FSE) density of an 18,650 cell is calculated as a more useful metric to compare an alloy electrode with graphite, with a baseline of 726Wh L^{-1}, as proposed by Obrovac et al. [11] The FSE density calculation is inversely related to the average voltage and directly related to the volumetric capacity, such that lower average voltage and higher volumetric capacity yields a higher FSE.

3. Results and discussion

3.1. Activity of elements

In general, the Li-activity of the pure elements in their amorphous phases tracks with that of the literature reports derived from calculations of the crystalline phases found on the ICSD and the Materials Project, as shown in Fig. 2. Deviations include C, Cu, Mg, Ca, Sr, and Ru. While the intercalation of Li into graphite is well studied, amorphous carbon is not as well understood. Dahn et al. estimate a maximum lithiation capacity corresponding to a-$Li_{0.5}C$ [43] which is enabled by lithiation of short-range graphitic environments. However, in our calculations, we find no capacity for a-C, which is attributed to the structural dissimilarity between our amorphous carbon structure and literature-reported a-C. Contrary to the disordered amalgamation of graphitic domains, our sampled a-C structures - formed through the melt-quench workflows - are comprised of layered amorphous graphene-like sheets which break down into carbon chains upon lithiation. Indeed, it is well-known that amorphous carbon capacity varies widely, depending on the degree and type of disorder [44–46]. It is generally accepted that Cu is inert; in fact, its electrochemical stability with respect to Li and high electronic conductivity have made it the most common anode current collectors [47]. However, within the Materials Project, a theoretical phase of tetragonal intermetallic $LiCu_3$ (mp-862658) is found to be stable at low temperatures. In addition, we find that the formation of amorphous intermetallic Cu-Li alloys to be stable relative to a-Cu and c-Li. Published Cu-Li phase diagrams observe solubility of Li in Cu at 23°C, up to $Li_{13}Cu_{87}$, and depicts the existence of a Cu_2Li_3 phase between ~ 500K-840K, although Cu_2Li_3 is predicted from temperature dependent EMF measurements, but was not directly observed in DTA or XRD studies and has, to date, no reported structure in the ICSD [48]. In support of this, Li interdiffusion with Cu is observed in several studies, however, only a few nanograms were found to diffuse over 28 days at room temperature [49]. This suggests that alloying reactions between Li and Cu are severely kinetically hindered. From Fig. S9, S14, and S31 we find no form stable amorphous Li-X phases forming with the Alkaline Earth metals (Mg, Ca, and Sr). Similarly, no stable crystalline Li-Sr phases are found. In contrast, multiple stable crystalline Li-Mg phases exist and one stable crystalline Li-Ca phase exists, although its(Li_2Ca) formation energy is only 12meV $atom^{-1}$. Li-Mg has been demonstrated to alloy with Li in experiments, however large capacity fade and low rate capability are observed, primarily attributed to the formation of high impedance surface films [11]. The Li_2Ca phase is reported in studies, however, the plating of Li metal is observed due to the low lithiation potentials of Ca [50]. While Obrovac et al. classify Ru as an active element, it is believed that the storage of Li does not occur through an alloying or intercalation mechanism [51]. Our calculations support this fact, finding no lithiation for amorphous or crystalline Ru.

A summary of electrochemical characteristics of the active elements are tabulated in Table 1. Most elements exhibit volumetric capacities 2-3x greater than graphite (850AhL^{-1}) [52] and consequently, most alloying strategies are expected to improve on the energy density of an 18,650 full cell, as compared to graphite. Notable exceptions include the Pnictogens (P, As, Sb), Chalcogens (O, S, Se, Te), and Halogens(F, Cl, Br, I) which exhibit lithiation potentials in excess of 1.0V vs Li/Li^+ due to

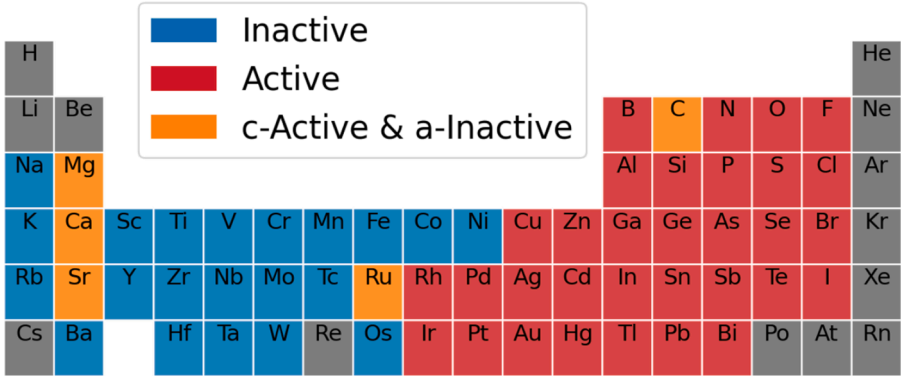

Fig. 2. Periodic table with the predicted active (blue) and inactive elements (red). Elements in orange form thermodynamically stable crystalline binary Li-X phases, but the amorphous phases are not predicted to lithiate. The elements in grey were not included in this study. (For interpretation of the references to colour in this figure legend, the reader is referred to the web version of this article.)

Table 1
Electrochemical Characteristics for all amorphous active elements.

	Max Volume Expansion (%)	Average Voltage (E)	Specific Capacity ($mAhg^{-1}$)	Volumetric Capacity (AhL^{-1})	FSE Improvement (%)
B	210	0.24	2480	1900	37
Al	300	0.089	2980	1880	43
P	250	0.56	3480	2110	27
S	50	1.7	2100	1770	-18
Cu	59	0.12	212	1120	28
Zn	100	0.27	410	1390	29
Ga	150	0.25	770	1710	34
Ge	310	0.25	1480	1940	37
As	180	0.69	1250	1960	21
Se	39	1.7	680	1450	-21
Br	-6	3.0	337	759	-73
Rh	310	0.13	781	2130	44
Pd	420	0.26	1010	2110	39
Ag	280	0.16	745	1850	40
Cd	220	0.12	715	1710	39
In	170	0.18	700	1680	36
Sn	260	0.25	1020	1870	36
Sb	190	0.54	880	1790	24
I	-15	2.4	212	569	-57
Te	54	1.4	421	1190	-14
Ir	200	0.26	279	1920	37
Pt	390	0.39	553	2150	34
Au	250	0.46	408	1940	29
Tl	200	0.12	525	1770	40
Pb	200	0.19	517	1740	37
Bi	180	0.43	516	1700	28

the formation of highly stable ionic compounds. In full cells, these elements would not yield a high potential difference and therefore would exhibit low energy density, evidenced by the negative full stack energy (FSE) improvement in Table 1.

Gaseous elements, such as H_2, N_2, O_2, and F_2, are omitted in Table 1, due to the lack of a well-defined solid-state reference and the difficulty in reporting derived quantities. In addition, materials prone to gas formation would require additional considerations to alleviate internal pressure and cell swelling. These chemistries, while impractical for anode materials, have been successfully used as cathode materials in systems such as lithium-sulfur or lithium-air batteries [53].

3.2. Binary and ternary si alloy formation

When alloying Si with another component, the ability of the two elements to mix and form stable binary alloys plays a significant role in the synthesis and performance of a material. When alloying with elements that form stable Si-X phases, synthesis of a phase-pure amorphous material may be relatively easy. The elements that do not form stable Si-X phases are immiscible and will tend to decompose into a composite of two elemental phases. Multiple thermodynamic and kinetic factors govern the formation of separated phases and domain size distribution. High interfacial energy will bias towards phase segregation and promote the formation of distinct Si and X regions while contributions to the free energy from the mixing entropy will stabilize mixtures. Conversely, low solid state diffusivities may inhibit the migration of alloy components, preventing structural transformation. Hence, due to these competing factors, careful modulation of synthesis and processing conditions related to cooling rate is necessary to control phase segregation. Non-equilibrium methods such as splat quenching, sputtering, and mechanical milling may form metastable Si alloys with near homogeneous elemental distributions. An example of this is the tuning of segregation in Si-Ge alloys through annealing temperature and sputtering time presented by Kim et al [54].

Alloys of immiscible components with more uniform element dispersions will exhibit an increased formation energy relative to their composite counterparts. Using the computed formation energy as a strong indicator of lithiation potential of the host alloy or more stable lithiated intermediates results, we surmise that the increased formation energy of homogeneous alloys will translate to an increased lithiation potential, in particular at early lithiation stages.

While phase segregation is not ideal, electrodes constructed from these materials have nevertheless shown improved performance. The formation of nanocomposites of two active elements via phase segregation during synthesis has shown improved cycling, as compared to Si, and the homogenization of these materials may even be seen after cycling [55].

The tendency for elements to form stable amorphous binary alloys, defined by the presence of at least one composition on the Si-X convex hull, with Si is shown in Fig. 3. Cross-referencing with the Li alloying activity (Fig. 2), we find that all inactive alloys are found to form stable crystalline Si-X phases. We find parity between the amorphous and crystalline when considering the Si-X phases, which are stable relative to their pure amorphous termini, except for C, Na, and K, for which no amorphous Si-X phases lie on the amorphous hull. In the active elements, we find B, C, and Au to form stable amorphous binary phases, but not crystalline.

Formation of a binary, however, does not preclude the phase decomposition during cycling. For chemical systems without stable ternaries, Si rich and Si poor regions may form during the alloy process with Li. Coarsening of these inhomogeneous regions is dependent on the diffusion kinetics, where fast diffusion will result in more pronounced phase separation. While Li diffusivity may be system dependent, in Si, diffusion is enhanced with Li alloying, reducing the barrier to growth of inhomogeneities [29,56]. While nanocomposite Si-M may be able to absorb stresses caused by inhomogeneous lithiation, larger regions may strain the material more, leading to stress induced cracking. In this regard, alloys that form many thermodynamically favorable ternary phases may be more stable, since they may undergo less drastic structural reorganization during lithiation and delithiation. Inclusion of all elements into a ternary would limit the separation of X and Si atoms to a few coordination shells.

Elements with unfavorable Si-X bonding which do not form binary phases do not form stable ternaries, here defined as a composition that forms a vertex on the amorphous hull. The energy above hull for these decreases with increased Li(example seen in SI fig S43 and S42, suggesting that Li buffers the repulsive interactions through the formation of Li-X and Li-Si bonds. The energy above hull is low enough that the entropic contributions to free energy may be sufficient to stabilize these ternaries near room temperature. At room temperature (23°C) the entropy of mixing, estimated using Boltzmann's equation, contributes up to 28meV $atom^{-1}$, therefore phases up to 28meV $atom^{-1}$ above the hull may be stable. Conversely, the favorability of Si-X bonds does not guarantee presence of a stable ternary phase as, for example, twelve of the elements which are miscible with Si do not form ternaries.

We find that a few elements exhibit a rich chemistry of ternary amorphous phases, including Ca, Cu, Ru, Rh, Pd, Ir, and Sr. In these systems, most calculated compositions do not deviate more than 10meV $atom^{-1}$ from the amorphous hull. We expect that these systems will exhibit featureless voltage curves, since there is no preferential phase/composition. This is indeed the case for $CaSi_2$, which is reported to have a featureless, sloping voltage curve [57]. The calculated discrete voltages, seen in fig. S72, for $Ca_{0.25}Si_{0.75}$ and $Ca_{0.5}Si_{0.5}$ show several lithiation voltage steps, each with relatively small capacities and we expect that - if many more amorphous compositions were sampled - a smooth, sloping lithiation profile would emerge.

3.3. Inactive alloys

Since all inactive elements are miscible with Si, the main differentiating factor in the evolution during lithiation is the ability to form ternary alloys. Two representative amorphous hulls for these two groups

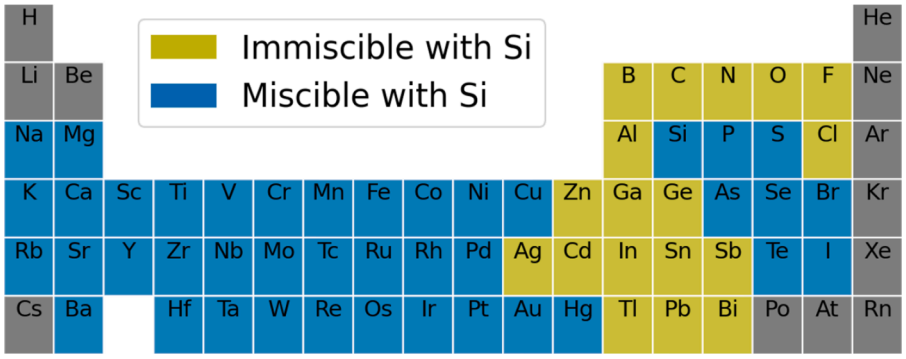

Fig. 3. Periodic table indicating the tendency for elements to form stable alloys or phases with Si. Elements with repulsive interactions with Si are shaded in blue, while those forming bonds with Si are filled green. (For interpretation of the references to colour in this figure legend, the reader is referred to the web version of this article.)

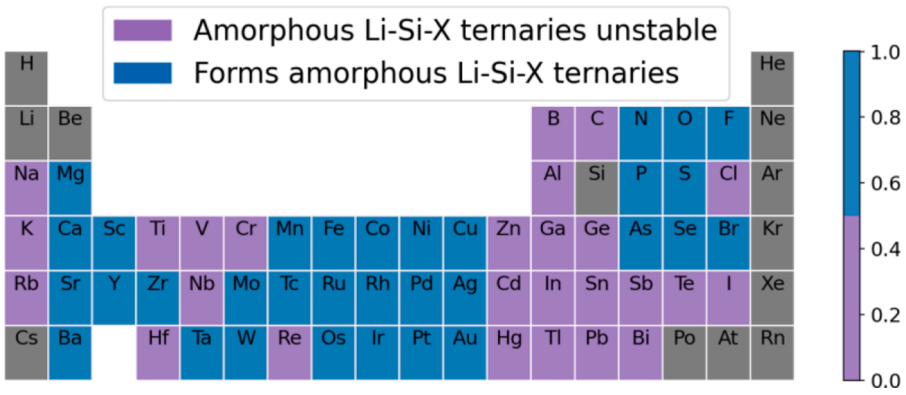

Fig. 4. Ternary phase formation with Li and Si. Elements which form stable ternary phases are colored in blue. Elements forming ternary compounds which all lie above the convex hull are shaded purple. We note that in some systems with stable ternaries, the ternaries are stabilized by only <5meV atom^{-1}. Caution should be exercised in interpreting this binary categorization, as numerical accuracy or entropy may destabilize the ternaries with respect to the binary alloys or pure elements. (For interpretation of the references to colour in this figure legend, the reader is referred to the web version of this article.)

of Si/inactive alloy systems are shown in Fig. 5 for the Cr-Si and Fe-Si systems, respectively.

Fig. 5 a is an example of an alloy component which forms binaries with Si, but does not form favorable amorphous ternary Li-Si-X phases. The two labeled composition ranges on the Si-Nb line correspond to:

- I-a) At low concentrations of alloyed inactive elements, the early lithiation potential will match those of Si, forming two phases - a Li-Si binary phase and Si-X phase. Once all Si has been exhausted, Li-Si phases will lithiate as usual, while the Si-X phase remains unchanged. When the composition intersects the $NbSi_2$-$Li_{26}Si_{15}$, lithiation further displaces more X rich Si-X phases. Lithiation depletes the Si in Si-X, until Nb_5Si_3 is reached, where no further lithiation is expected due to the two phase equilibrium with BCC Li.
- II-a) No lithiation is expected for alloys with composition falling within this range. Because there are no nodes on the Li-Nb phase equilibrium line, no Nb is not expected to lithiate. Additionally, these phase equilibrium triangles predict a equilibria with Li, no capacity is expected since Li plating is more favorable than Li alloying.

the boundary between I-a and II-a varies among the inactive elements as well as for the amorphous and crystalline materials. Generally, alloying with X $z \geq 50$ will yield little to no capacity and should be avoided. Based on our findings, we do not recommend alloying with more than 33-40atom % of these inactive elements, since capacity is significantly penalized above this composition.

Fig. 5b depicts an alloying element for which the of binary and ternary amorphous phases are predicted to form. The formation of ternaries may be able to extend the range of alloys with lithiation capacity. In these systems, the lithiation is bounded by the formation of the ternary Li-Si-X phase rather than a Si-X binary. While inactive components are not expected to contribute capacity and bind Si active material, the formation of a ternary phase results in additional Li storage when compared to those which do not form a ternary. In the case of Fe, the formation of $LiFe_2Si$, additional capacity is observed in Fe rich $Si_{1-z}Fe_z$ alloys (II-b in Fig. 5), as some metal is reduced and extruded. Comparing Si-Fe to Si-Nb, an alloy with composition Nb_2Si would not alloy with Li while Fe_2Si stores one Li per host formula unit.

In both phase diagrams in Fig. 5, it is clear that the alloyed inactive metals do not get fully reduced and displaced, favoring the formation of intermediate binaries or ternaries, consuming Si active material. In the case of Nb, Nb_5Si_3 is formed as an inert matrix and continued cycling proceeds alloying (and dealloying) of the Li-Si binaries. It is commonly cited that alloys derived from inactive elements do not actively participate in compound formation with Li [11,20] and follow the reaction shown in Eqs. (4) and (5).

First lithiation:

$$X_zSi_{1-z} + n(1-z)Li^+ + n(1-z)e^- \longrightarrow (1-z)Li_nSi + zX \quad (4)$$

Subsequent cycling:

$$Li_nSi + X \longleftrightarrow Si + X + nLi^+ + ne^- \quad (5)$$

For an alloy to follow this chemical reaction, its corresponding phase diagram must show an equilibrium between X, Li, and an Li-Si phase. Thus, the Si-X binary phases must have a higher formation energy (less stable) than the Li-Si phases. In our calculations, the methodology for sampling amorphous configurations provides an upper bound on the formation energy, where more sampling statistics can only decrease formation energy. Therefore, in most of the inactive alloy systems, the Li-Si alloys will always be more stable than the Si-X alloys. Amorphous

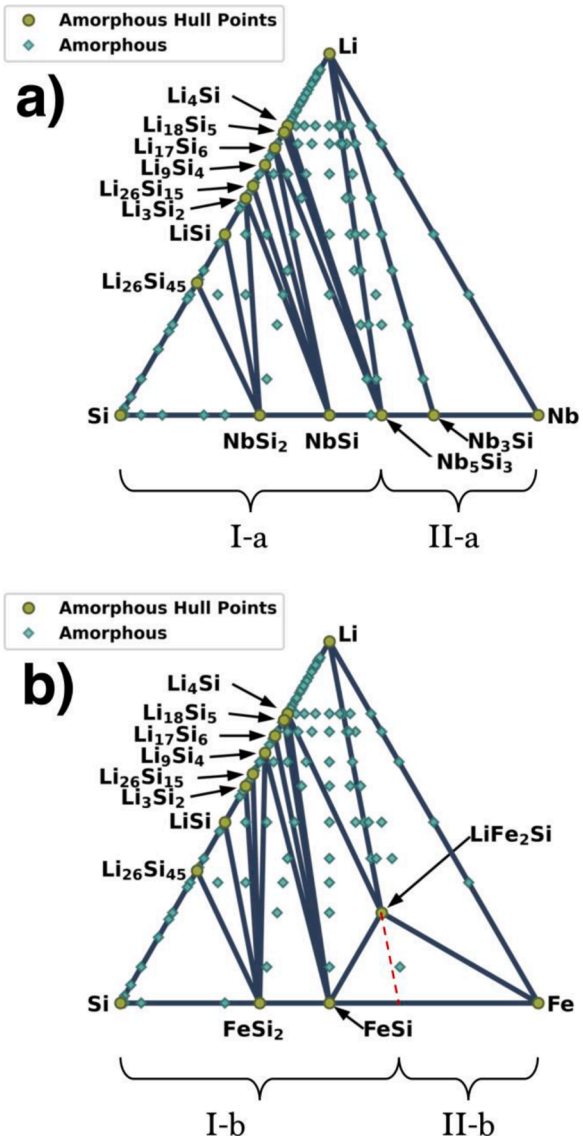

Fig. 5. Sample amorphous hulls for Si/inactive alloys depicting chemical systems with a) no stable ternaries and b) stable ternaries formed. Stable and unstable phases are represented by green circles and teal diamonds, respectively. Red dashed line in b) is a projection of the Li-$LiFe_2Si$ tie-line and its intersection with the Si-Fe equilibrium is the cutoff between I-b and II-b. (For interpretation of the references to colour in this figure legend, the reader is referred to the web version of this article.)

Mn_zSi_{1-z} is the only system found, among the amorphous and crystalline Si-X, to completely extrude Mn metal and is shown in Fig. 6. In this system, lithiation is bounded by the Li-M-Li_4Si equilibrium with a final lithiation state coincident with the M-Li_4Si tie-line. More accurate chemical reactions to describe most Si/inactive alloy materials are shown in Eqs. (6) and (7):

First lithiation:

$$X_nSi_y + \delta nLi^+ + \delta ne^- \rightarrow \delta Li_nSi + X_nSi_{(y-\delta)} \quad (6)$$

Subsequent cycling:

$$Li_nSi + X_nSi_{(y-\delta)} \leftrightarrow Si + X_nSi_{(y-\delta)} + nLi^+ + ne^- \quad (7)$$

where the inactive element deactivates Si active material through the formation of X rich binary alloys. Upon delithiation, Si may not quickly re-alloy with the inactive Si-X phase extruded, due to the sluggish kinetics for Si diffusion. In support of this, Yang et al. reported electro-

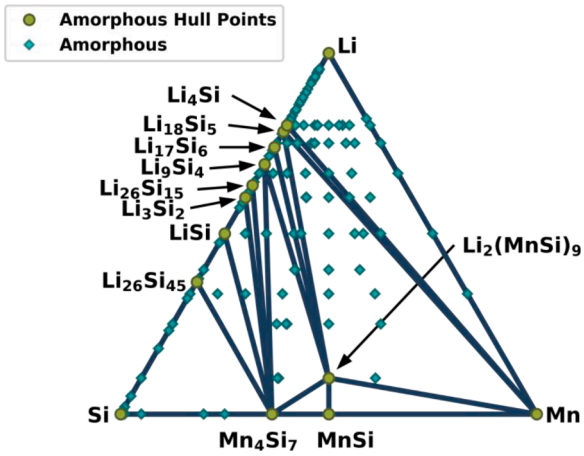

Fig. 6. Li-Mn-Si phase diagram showing the only system tending to extrude pure metal. Any $Mn_zSi_{(1-z)}$ material will intersect the Mn-Li_4Si phase equilibrium and displace Mn metal.

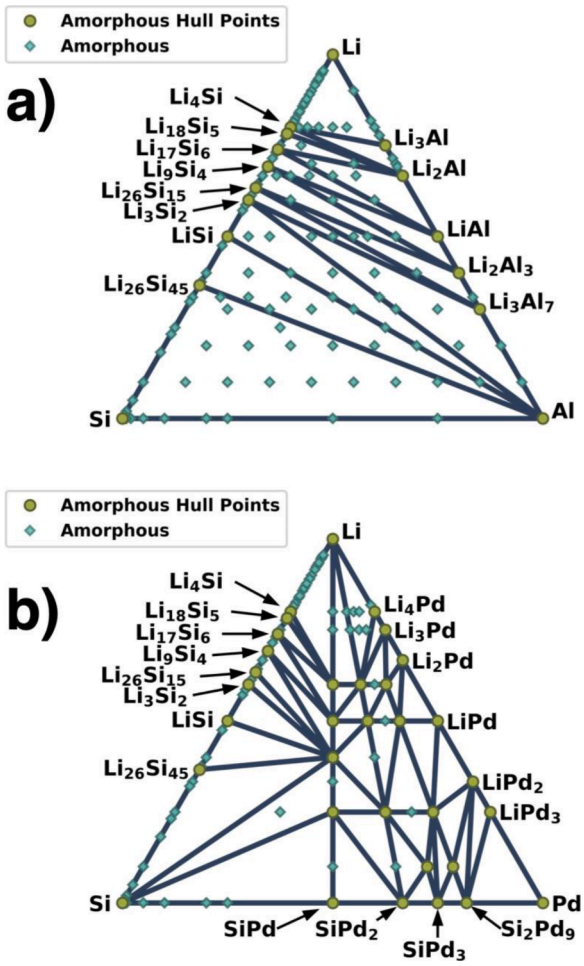

Fig. 7. Sample amorphous hulls for Si/active alloys depicting chemical systems which are a) immiscible and do not form stable ternaries b) miscible and form stable ternaries. Stable and unstable phases are represented by green circles and teal diamonds, respectively. (For interpretation of the references to colour in this figure legend, the reader is referred to the web version of this article.)

chemically inactive $NiSi_x$ nanowires coated with Si which cycled reversibly without affecting the $NiSi_x$ core [58,59].

Therefore, decreased average voltage seen when alloying inactive

elements may be attributed to two contributions. i) Decreased volumetric expansion as proposed by Obrovac et al.[19] This is similar to the mechanism proposed by Obrovac et al.[22], however the volumetric expansion is buffered by irreversible X_zSi_{1-z} phases rather than X. ii) Electrodes constructed from materials with higher X concentration than $\sim$ 33% will bypass early Li_nSi $(0 \leq n \leq 1.5)$ lithiation stages and start at a lower potential.

3.4. Active alloys

The majority of Si/active systems fall into two groups: 1) elements which are immiscible with Si and do not form stable ternary phases or 2) elements that are miscible with Si and do form stable ternary phases. Only a handful of ternary alloy systems fall outside of these two groups. Ag is the only active element that is immiscible with Si and form stable amorphous ternaries. Te, I, and Hg are all miscible with Si, but do not form stable amorphous ternaries.

Immiscible alloy components will have a high driving force for phase segregation, especially those with no ternaries. Thus, those in group 1) will tend to form a nanocomposite during synthesis, unless kinetics are significantly hindered through high quenching rate or ball milling. Alloys synthesized through this method may be highly metastable, even relative to the amorphous hull. These alloys will exhibit an increased lithiation potential during the first lithiation, along with formation of two distinct lithiation phases (one Li-X and Li-Si). In subsequent cycling, the two lithiated phases will cycle as expected for each of Li-X and Li-Si. In some of these alloys, homogeneous lithiated phases lie closer to the hull, where the entropy may be sufficient to stabilize the alloy near room temperature and phase segregation may not be observed. The tie-triangles composing the lithiation pathway followed for these materials always share an edge with Li-Si or Li-X and therefore the lithiation potential is a composite of the Si and X lithiation potentials. Because alloying with these active elements does not form irreversible phases, any Si/active alloy composition may be suitable for active materials. For highest specific capacity, a higher Si content is desirable, while for volumetric capacity it is element dependent, since some elements have comparable volumetric capacities to Si.

Materials within group (ii) should theoretically form materials with higher mechanical stability during cycling. The absence of two distinct phases during lithiation may give rise to more uniform stress distributions due to uniform lithium distribution. Many precious or rare elements, such as Pd, Rh, Pt, and Ir, which may not be practical for use in Li-ion batteries fall under this group. Early lithiation potentials in Pt and Pd based alloys are rather high ($>$ 0.8V vs Li/Li^+), while Rh and Ir exhibit more useful potentials ($\sim$ 0.55V vs Li/Li^+). Also in this group are the aforementioned elements which form highly stable compounds with Li, such O, S, Te, and Sb. While these elements do not have direct utility as anodes, they may be used in a manner similar to the inactive alloys. During the first lithiation cycle of binary Si alloys containing these elements, very stable ternary and binary phases will be formed at high potentials ($>$ 1.0V vs Li/Li^+). These phases will be functionally irreversible phases and may not actively participate in any reactions and would serve as a buffering matrix to accommodate stress and decrease volumetric expansion. In the case of SiO_x, cycling is found to form a Li-ion conductive Li_4SiO_4 phase during lithiation which is not associated with a large volume expansion [29,60,61]. Fast charge transfer at the SiO/electrolyte interface is also found, signaling that alloying with these high voltage elements may improve the rate capability of electrodes. Although these phases may be inert within the range of cycling, it is important to remember that they deplete Li inventory. Given that current cathodes are the source of Li in newly manufactured batteries, this decreases the effective reversible cathode capacity, requiring considerations such as a higher ratio of cathode to anode capacity or prelithiation of the anode [10,62]. Zhao et al. reported on a Li_xSi/Li_2O composite anode synthesized through metallurgical prelithiation of SiO_x with $\sim$ 99.87% coulombic efficiency over 400 cycles [63].

4. Conclusion

In summary, we conduct an ab-initio investigation of the thermodynamic impact of alloying Si with a second component. We find that inactive components do not get fully displaced to form pure metals as literature reaction mechanisms propose. Instead, stable Si-X phases are formed which do not lithiate, binding otherwise active Si in an inactive phase which is detrimental to capacity. This results in higher capacity loss than would be expected for a non-participating additive. Si/inactive alloys, however, are capable of bypassing higher voltage Si lithiation stages, thereby decreasing the average potential and increasing energy density. A subset of Si/active alloys are found to favor phase separation to form nanocomposite materials which match the lithiation potentials of the individual alloy components. The remaining Si/active elements will displace stable ionic compounds when reacting with Li, which are functionally irreversible due to high (de)lithiation potential($\geq$ 1.0V vs Li/Li^+). These may be function in a similar manner to inactive phases in Si/inactive alloys, although they deplete Li inventory rather than Si active material. While we have focused on binary Si-X alloys, the methods and analysis we have utilized to model amorphous materials and predict their electrochemical characteristics may be generalized for more alloyed components (ternary, quaternary, etc.) to rapidly screen the chemical space for Si-based alloy electrodes.

CRediT authorship contribution statement

Eric Sivonxay: Conceptualization, Methodology, Data curation, Writing – original draft, Software, Validation. **Kristin A. Persson:** Conceptualization, Methodology, Supervision, Writing – review & editing.

Declaration of Competing Interest

The authors declare that they have no known competing financial interests or personal relationships that could have appeared to influence the work reported in this paper.

Data availability

Data will be made available on request.

Acknowledgements

This work was supported in part by the Advanced Battery Materials Research (BMR) program directed by Tien Duong and in part by the U.S. Department of Energy's Vehicle Technologies Office under the Silicon Consortium Project, directed by Brian Cunningham, and managed by Anthony Burrell. This research utilized resources at the National Energy Research Scientific Computing Center (NERSC), a U.S. Department of Energy Office of Science User Facility located at Lawrence Berkeley National Laboratory and the Lawrencium computational cluster resource provided by the IT Division at the Lawrence Berkeley National Laboratory, operated under Contract No. DE-AC02-05CH11231. Additionally, a portion of this research was performed using computational resources sponsored by the Department of Energy's Office of Energy Efficiency and Renewable Energy and located at the National Renewable Energy Laboratory (NREL). We gratefully acknowledge Shyam Dwaraknath and Jianli Cheng for valuable discussion.

Supplementary material

Supplementary material associated with this article can be found, in the online version, at doi:10.1016/j.ensm.2022.08.015.

References

[1] Y. Zhao, O. Pohl, A.I. Bhatt, G.E. Collis, P.J. Mahon, T. Rüther, A.F. Hollenkamp, A review on battery market trends, second-Life reuse, and recycling, Sustain. Chem. 2 (1) (2021) 167–205, https://doi.org/10.3390/suschem2010011.

[2] Global ev outlook 2020, 2020, https://www.iea.org/reports/global-ev-outlook-2020.

[3] C. Xu, Q. Dai, L. Gaines, M. Hu, A. Tukker, B. Steubing, Future material demand for automotive lithium-based batteries, Commun. Mater. 1 (1) (2020), https://doi.org/10.1038/s43246-020-00095-x.

[4] M.S. Whittingham, Ultimate limits to intercalation reactions for lithium batteries, Chem. Rev. 114 (23) (2014) 11414–11443, https://doi.org/10.1021/cr5003003.

[5] C. Chan, H. Peng, G. Liu, K. McIlwrath, X. Zhang, R. Huggins, Y. Cui, High-performance lithium battery anodes using silicon nanowires, Nat. Nanotechnol. 3 (1) (2007) 31–35, https://doi.org/10.1038/nnano.2007.411.

[6] H.-H. Chiang, J.-M. Lu, C.-L. Kuo, First-principles study of the structural and dynamic properties of the liquid and amorphous li-Si alloys, J. Chem. Phys. 144 (3) (2016) 034502, https://doi.org/10.1063/1.4939716.

[7] B. Key, R. Bhattacharyya, M. Morcrette, V. Seznec, J.M. Tarascon, C.P. Grey, Real-time NMR investigations of structural changes in silicon electrodes for lithium-ion batteries, J. Am. Chem. Soc. 131 (26) (2009) 9239–9249, https://doi.org/10.1021/ja8086278.

[8] J. Li, J.R. Dahn, An in situ X-Ray diffraction study of the reaction of li with crystalline si, J. Electrochem. Soc. 154 (3) (2007) A156, https://doi.org/10.1149/1.2409862.

[9] Y. Yin, E. Arca, L. Wang, G. Yang, M. Schnabel, L. Cao, C. Xiao, H. Zhou, P. Liu, J. Nanda, G. Teeter, B. Eichhorn, K. Xu, A. Burrell, C. Ban, Nonpassivated silicon anode surface, ACS Appl. Mater. Interfaces 12 (23) (2020) 26593–26600, https://doi.org/10.1021/acsami.0c03799.

[10] F. Zhang, J. Yang, Boosting initial coulombic efficiency of si-based anodes: a review, Emerg. Mater. 3 (3) (2020) 369–380, https://doi.org/10.1007/s42247-020-00080-7.

[11] M.N. Obrovac, V.L. Chevrier, Alloy negative electrodes for li-ion batteries, Chem. Rev. 114 (23) (2014) 11444–11502, https://doi.org/10.1021/cr500207g.

[12] Y. Jin, B. Zhu, Z. Lu, N. Liu, J. Zhu, Challenges and recent progress in the development of si anodes for lithium-ion battery, Adv. Energy Mater. 7 (23) (2017), https://doi.org/10.1002/aenm.201700715.

[13] K. Rhodes, N. Dudney, E. Lara-Curzio, C. Daniel, Understanding the degradation of silicon electrodes for lithium-Ion batteries using acoustic emission, J. Electrochem. Soc. 157 (12) (2010) A1354, https://doi.org/10.1149/1.3489374.

[14] B. Han, C. Liao, F. Dogan, S.E. Trask, S.H. Lapidus, J.T. Vaughey, B. Key, Using mixed salt electrolytes to stabilize silicon anodes for lithium-Ion batteries via in situ formation of li-M-Si ternaries (m = mg, zn, al, ca), ACS Appl. Mater. Interfac. 11 (2019) 29780–29790, https://doi.org/10.1021/acsami.9b07270.

[15] Y. Zhang, X. Li, E. Sivonxay, J. Wen, K.A. Persson, J.T. Vaughey, B. Key, F. Dogan, Silicon anodes with improved calendar life enabled by multivalent additives, Adv. Energy Mater. (2021), https://doi.org/10.1002/aenm.202101820.

[16] M. Schnabel, T.C. Lin, E. Arca, I. Yoon, G.M. Veith, X. He, R. Kostecki, Stable SEI formation on al-Si-Mn metallic glass li-Ion anode, J. Electrochem. Soc. 168 (10) (2021) 100521, https://doi.org/10.1149/1945-7111/ac2d3f.

[17] J. Xu, M. Ling, L. Terborg, H. Zhao, F. Qiu, J.J. Urban, R. Kostecki, G. Liu, W. Tong, Facile synthesis and electrochemistry of si-Sn-C nanocomposites for high-Energy li-Ion batteries, J. Electrochem. Soc. 164 (7) (2017) A1378–A1383, https://doi.org/10.1149/2.0241707jes.

[18] T.D. Hatchard, J.M. Topple, M.D. Fleischauer, J.R. Dahn, Electrochemical performance of sialsn films prepared by combinatorial sputtering, Electrochem. Solid-State Lett. 6 (7) (2003) 129–132, https://doi.org/10.1149/1.1574231.

[19] M.N. Obrovac, L. Christensen, D.B. Le, J.R. Dahn, Alloy design for lithium-ion battery anodes, J. Electrochem. Soc. 154 (9) (2007) 849–855, https://doi.org/10.1149/1.2752985.

[20] B. Ding, Z. Cai, Z. Ahsan, Y. Ma, S. Zhang, G. Song, C. Yuan, W. Yang, C. Wen, A review of metal silicides for lithium-Ion battery anode application, Acta Metallurgica Sinica (English Lett.) 34 (3) (2021) 291–308, https://doi.org/10.1007/s40195-020-01095-z.

[21] H. Kim, J. Choi, H. Sohn, T. Kang, The insertion mechanism of lithium into mg2si anode material for li–Ion batteries, J. Electrochem. Soc. 146 (12) (1999) 4401–4405, https://doi.org/10.1149/1.1392650.

[22] M.N. Obrovac, L.J. Krause, Reversible cycling of crystalline silicon powder, J. Electrochem. Soc. 154 (2) (2007) A103, https://doi.org/10.1149/1.2402112.

[23] A. Inoue, High strength bulk amorphous alloys with low critical cooling rates (overview), Mater. Trans., JIM 36 (7) (1995) 866–875, https://doi.org/10.2320/matertrans1989.36.866.

[24] W.L. Johnson, Bulk amorphous metal-An emerging engineering material, Jom 54 (3) (2002) 40–43, https://doi.org/10.1007/BF02822619.

[25] M. Chen, A brief overview of bulk metallic glasses, NPG Asia Mater. 3 (9) (2011) 82–90, https://doi.org/10.1038/asiamat.2011.30.

[26] Z.y. Feng, W.j. Peng, Z.x. Wang, H.j. Guo, X.h. Li, G.c. Yan, J.x. Wang, Review of silicon-based alloys for lithium-ion battery anodes, Int. J. Miner. Metallur. Mater. 28 (10) (2021) 1549–1564, https://doi.org/10.1007/s12613-021-2335-x.

[27] A. Jain, S.P. Ong, G. Hautier, W. Chen, W.D. Richards, S. Dacek, S. Cholia, D. Gunter, D. Skinner, G. Ceder, K.A. Persson, Commentary: the materials project: a materials genome approach to accelerating materials innovation, APL Mater. 1 (1) (2013), https://doi.org/10.1063/1.4812323.

[28] N. Nitta, G. Yushin, High-capacity anode materials for lithium-ion batteries: choice of elements and structures for active particles, Part. Part. Syst. Char. 31 (3) (2014) 317–336, https://doi.org/10.1002/ppsc.201300231.

[29] E. Sivonxay, M. Aykol, K.A. Persson, The lithiation process and li diffusion in amorphous sio2 and si from first-principles, Electrochim. Acta 331 (xxxx) (2020) 135344, https://doi.org/10.1016/j.electacta.2019.135344.

[30] M. Aykol, S.S. Dwaraknath, W. Sun, K.A. Persson, Thermodynamic limit for synthesis of metastable inorganic materials, Sci. Adv. 4 (4) (2018) eaaq0148, https://doi.org/10.1126/sciadv.aaq0148.

[31] K. Mathew, J.H. Montoya, A. Faghaninia, S. Dwarakanath, M. Aykol, H. Tang, I.-H. Chu, T. Smidt, B. Bocklund, M. Horton, J. Dagdelen, B. Wood, Z.-K. Liu, J. Neaton, S.P. Ong, K. Persson, A. Jain, Atomate: a high-level interface to generate, execute, and analyze computational materials science workflows, Comput. Mater. Sci 139 (2017) 140–152, https://doi.org/10.1016/j.commatsci.2017.07.030.

[32] A. Jain, S.P. Ong, W. Chen, B. Medasani, X. Qu, M. Kocher, M. Brafman, G. Petretto, G.-M. Rignanese, G. Hautier, D. Gunter, K.A. Persson, Fireworks: a dynamic workflow system designed for high-throughput applications, Concurr. Comput. 27 (17) (2015) 5037–5059, https://doi.org/10.1002/cpe.3505.

[33] S.P. Ong, W.D. Richards, A. Jain, G. Hautier, M. Kocher, S. Cholia, D. Gunter, V. L. Chevrier, K.A. Persson, G. Ceder, Python materials genomics (pymatgen): a robust, open-source python library for materials analysis, Comput. Mater. Sci 68 (2013) 314–319, https://doi.org/10.1016/j.commatsci.2012.10.028.

[34] F. Birch, Finite elastic strain of cubic crystals, Phys. Rev. 71 (11) (1947) 809–824, https://doi.org/10.1103/PhysRev.71.809.

[35] F.D. Murnaghan, Physics: f. d. murnaghan (1944) 244–247.

[36] G. Kresse, J. Furthmüller, Efficiency of ab-initio total energy calculations for metals and semiconductors using a plane-wave basis set, Comput. Mater. Sci 6 (1) (1996) 15–50, https://doi.org/10.1016/0927-0256(96)00008-0.

[37] G. Kresse, J. Furthmüller, Efficient iterative schemes for ab initio total-energy calculations using a plane-wave basis set, Phys. Rev. B - Condens. Matter Mater. Phys. 54 (16) (1996) 11169–11186, https://doi.org/10.1103/PhysRevB.54.11169.

[38] P.E. Blöchl, Projector augmented-wave method, Phys. Rev. B 50 (24) (1994) 17953–17979, https://doi.org/10.1103/PhysRevB.50.17953.

[39] J.P. Perdew, K. Burke, M. Ernzerhof, Generalized gradient approximation made simple, Phys. Rev. Lett. 77 (18) (1996) 3865–3868, https://doi.org/10.1103/PhysRevLett.77.3865.

[40] L. Wang, T. Maxisch, G. Ceder, Oxidation energies of transition metal oxides within the GGA+u framework, Phys. Rev. B - Condens. Matter Mater. Phys. 73 (19) (2006) 1–6, https://doi.org/10.1103/PhysRevB.73.195107.

[41] S.P. Ong, L. Wang, B. Kang, G. Ceder, Li - Fe - P - O2 phase diagram from first principles calculations, Chem. Mater. 20 (5) (2008) 1798–1807, https://doi.org/10.1021/cm702327g.

[42] A. Van Der Ven, Z. Deng, S. Banerjee, S.P. Ong, Rechargeable alkali-Ion battery materials: theory and computation, Chem. Rev. 120 (14) (2020) 6977–7019, https://doi.org/10.1021/acs.chemrev.9b00601.

[43] J.R. Dahn, R.E. Mar, A. Abouzeid, Combinatorial study of sn[sub 1-x]co[sub x] (0<x<0.6) and [Sn[sub 0.55]co[sub 0.45]][sub 1-y]c[sub y] (0<y<0.5) alloy negative electrode materials for li-Ion batteries, J. Electrochem. Soc. 153 (2) (2006) A361, https://doi.org/10.1149/1.2150160.

[44] J. Robertson, Amorphous carbon, Adv. Phys. 35 (4) (1986) 317–374, https://doi.org/10.1080/00018738600101911.

[45] M.P. Ho, A.K. Lau, Amorphous carbon nanocomposites, Filler. Reinforcemenr Adv. Nanocompos. (2) (2015) 309–328, https://doi.org/10.1016/B978-0-08-100079-3.00012-0.

[46] S.C. Ray, Introduction: carbon and carbon nanomaterials, Magnetism Spintronic. Carbon Carbon Nanostruct. Mater. (2020) 23–45, https://doi.org/10.1016/b978-0-12-817680-1.00002-0.

[47] J. Asenbauer, T. Eisenmann, M. Kuenzel, A. Kazzazi, Z. Chen, D. Bresser, The success story of graphite as a lithium-ion anode material – fundamentals, remaining challenges, and recent developments including silicon (oxide) composites, Sustain. Energy Fuels 4 (11) (2020) 5387–5416, https://doi.org/10.1039/D0SE00175A.

[48] H. Okamoto, Cu-Li (copper-Lithium), J. Phase Equilibr. Diffus. 32 (2) (2011) 172, https://doi.org/10.1007/s11669-010-9840-3.

[49] R. Rupp, B. Caerts, A. Vantomme, J. Fransaer, A. Vlad, Lithium diffusion in copper, J. Phys. Chem. Lett. 10 (17) (2019) 5206–5210, https://doi.org/10.1021/acs.jpclett.9b02014.

[50] W. Jia, Z. Wang, J. Li, X. Yu, Y. Wei, Z. Yao, Y. Liu, Y. Wang, A. Zhou, W. Zou, F. Zhou, H. Li, A dual-phase li-Ca alloy with a patternable and lithiophilic 3D framework for improving lithium anode performance, J. Mater. Chem. A 7 (39) (2019) 22377–22384, https://doi.org/10.1039/c9ta08798b.

[51] Y. Kim, J.H. Um, H. Lee, W. Choi, W.I. Choi, H.S. Lee, O.H. Kim, J.M. Kim, Y. H. Cho, W.S. Yoon, Additional lithium storage on dynamic electrode surface by charge redistribution in inactive ru metal, Small 16 (1) (2020) 1905868, https://doi.org/10.1002/smll.201905868.

[52] R. Mo, X. Tan, F. Li, R. Tao, J. Xu, D. Kong, Z. Wang, B. Xu, X. Wang, C. Wang, J. Li, Y. Peng, Y. Lu, Tin-graphene tubes as anodes for lithium-ion batteries with high volumetric and gravimetric energy densities, Nat. Commun. 11 (1) (2020) 1–11, https://doi.org/10.1038/s41467-020-14859-z.

[53] A. Ulvestad, H.F. Andersen, I.J. Jensen, T.T. Mongstad, J.P. Maehlen, O. Prytz, M. Kirkengen, Substoichiometric silicon nitride - An anode material for li-ion batteries promising high stability and high capacity, Sci. Rep. 8 (1) (2018) 1–13, https://doi.org/10.1038/s41598-018-26769-8.

[54] H. Kim, Y. Son, C. Park, M.J. Lee, M. Hong, J. Kim, M. Lee, J. Cho, H.C. Choi, Germanium silicon alloy anode material capable of tunable overpotential by nanoscale si segregation, Nano Lett. 15 (6) (2015) 4135–4142, https://doi.org/10.1021/acs.nanolett.5b01257.

[55] K. Yao, M. Ling, G. Liu, W. Tong, Chemical reduction synthesis and electrochemistry of si-Sn nanocomposites as high-Capacity anodes for li-Ion

batteries, J. Phys. Chem. Lett. 9 (17) (2018) 5130–5134, https://doi.org/10.1021/acs.jpclett.8b02066.
[56] P. Johari, Y. Qi, V.B. Shenoy, The mixing mechanism during lithiation of si negative electrode in li-ion batteries: an ab initio molecular dynamics study, Nano Lett. 11 (12) (2011) 5494–5500, https://doi.org/10.1021/nl203302d.
[57] J. Wolfenstine, Casi2 as an anode for lithium-ion batteries, J. Power Sourc. 124 (1) (2003) 241–245, https://doi.org/10.1016/S0378-7753(03)00731-6.
[58] K. Kang, K. Song, H. Heo, S. Yoo, G.S. Kim, G. Lee, Y.M. Kang, M.H. Jo, Kinetics-driven high power li-ion battery with A-Si/nisix core-shell nanowire anodes, Chem. Sci. 2 (6) (2011) 1090–1093, https://doi.org/10.1039/c0sc00628a.
[59] N. Du, X. Fan, J. Yu, H. Zhang, D. Yang, Ni3si2-Si nanowires on ni foam as a high-performance anode of li-ion batteries, Electrochem. Commun. 13 (12) (2011) 1443–1446, https://doi.org/10.1016/j.elecom.2011.09.017.
[60] T. Kim, S. Park, S.M. Oh, Solid-State NMR and electrochemical dilatometry study on li[sup +] uptake/extraction mechanism in SiO electrode, J. Electrochem. Soc. 154 (12) (2007) A1112, https://doi.org/10.1149/1.2790282.
[61] M.A. Al-Maghrabi, J. Suzuki, R.J. Sanderson, V.L. Chevrier, R.A. Dunlap, J. R. Dahn, Combinatorial studies of $Si_{1-x}O_x$ as a potential negative electrode material for li-Ion battery applications, J. Electrochem. Soc. 160 (9) (2013) A1587–A1593, https://doi.org/10.1149/2.115309jes.
[62] F. Wang, B. Wang, J. Li, B. Wang, Y. Zhou, D. Wang, H. Liu, S. Dou, Prelithiation: A Crucial strategy for boosting the practical application of next-Generation lithium ion battery, ACS Nano 15 (2) (2021) 2197–2218, https://doi.org/10.1021/acsnano.0c10664.
[63] J. Zhao, H.-W. Lee, J. Sun, K. Yan, Y. Liu, W. Liu, Z. Lu, D. Lin, G. Zhou, Y. Cui, Metallurgically lithiated siox anode with high capacity and ambient air compatibility, Proc. Natl. Acad. Sci. 113 (27) (2016) 7408–7413, https://doi.org/10.1073/pnas.1603810113.